Assessing complex aeolian dune field morphology and evolution with Sentinel-1 SAR imagery-Possibilities and limitations

Bruno Boemke, Imen Turki, Catrina Bruell, Frank Lehmkuhl

▶ **To cite this version:**

Bruno Boemke, Imen Turki, Catrina Bruell, Frank Lehmkuhl. Assessing complex aeolian dune field morphology and evolution with Sentinel-1 SAR imagery-Possibilities and limitations. Aeolian Research, 2023, 62, 10.1016/j.aeolia.2023.100876 . hal-04290109

HAL Id: hal-04290109
https://hal.science/hal-04290109

Submitted on 20 Nov 2023

HAL is a multi-disciplinary open access archive for the deposit and dissemination of scientific research documents, whether they are published or not. The documents may come from teaching and research institutions in France or abroad, or from public or private research centers.

L'archive ouverte pluridisciplinaire **HAL**, est destinée au dépôt et à la diffusion de documents scientifiques de niveau recherche, publiés ou non, émanant des établissements d'enseignement et de recherche français ou étrangers, des laboratoires publics ou privés.

Distributed under a Creative Commons Attribution - NonCommercial - NoDerivatives 4.0 International License

Aeolian Research 62 (2023) 100876

Contents lists available at ScienceDirect

Aeolian Research

journal homepage: www.elsevier.com/locate/aeolia

Assessing complex aeolian dune field morphology and evolution with Sentinel-1 SAR imagery – Possibilities and limitations

Bruno Boemke [a,*], Imen Turki [b], Catrina Brüll [c], Frank Lehmkuhl [a]

[a] Department of Geography, RWTH Aachen University, Aachen, Germany
[b] Univ Rouen Normandie, Univ Caen Normandie, CNRS, M2C, UMR 6143, Rouen, France
[c] Institute of Hydraulic Engineering and Water Resources Management, RWTH Aachen University, Aachen, Germany

ARTICLE INFO

Keywords:
Sentinel-1 satellite imagery
Google Earth Engine
Aeolian dunes
Dune morphology
Continuous wavelet transform
Multi-timescale variability

ABSTRACT

Aeolian dune movement poses a threat to critical infrastructure, urban areas, water resources as well as agriculture. This threat is expected to increase in the coming years due to land degradation, desertification and climate change. Several approaches have been used to investigate the evolution of dune fields. Satellite remote sensing can be considered one of the most accurate tools for the continuous monitoring of global sand covered surfaces. Although early studies found a great potential in synthetic aperture radar (SAR) for dune assessment, the full potential has not been explored as of yet. Therefore, in this study, we present a novel method for assessing complex dune field morphology based on the easily accessible and globally available Sentinel-1 ground range detected (GRD) SAR dataset. In this application, dune features are extracted based on backscatter properties related to the local incidence angle. This provides a clear identification of (1) active dune sand, (2) dune ridges and (3) inter-dune ripples. By extracting these features through profiles, the multi-timescale evolution of the Western Mongolian dune field Bor Khyar was analysed through three areas of interest (AOIs) based on the spectral technique of continuous wavelets. The result of this investigation gives new insights into the temporal and spatial dynamics of dunes scale and their response to aeolian activity, revealing differences in aeolian activity as well as inter- and intra-annual variations in the dune morphology. These results are promising and highlight the potential in using satellite SAR imagery for dune monitoring.

Introduction

15% of the world's surface is covered by arid regions, of which approximately one third is mantled by sand deposits (Thomas 2011). In these regions, aeolian transport processes favour dune movement, posing a potential threat to critical infrastructure, urban areas, water resources as well as agriculture. Recent well documented examples for the hazardous aspects of aeolian transport can be found in the Nile region (El Gammal and El Gammal 2010; Eljack et al. 2010; Verstraeten et al. 2014; Saad et al. 2018), Western Asia (Al-Ghamdi and Hermas 2015; Pradhan et al. 2018; Amin and Seif 2019) as well as Western Africa (Ikazaki 2015; Benjaminsen and Hiernaux 2019; Yang et al. 2022). Due to land degradation, desertification and ongoing climate change, this threat is expected to increase dramatically and to occur in additional regions worldwide in the coming years (Davies et al. 2015; Reed and Stringer 2015; Shukla et al. 2019).

A continuous monitoring of sand covered surfaces is crucial to access the risk that desertification and related processes pose and ensure sustainable development in arid regions. Due to difficulties in accessibility of dune fields, field studies in these landscapes are often limited in their spatial coverage and associated with high costs. Satellite remote sensing, however, can cover large areas systematically, repetitively, and at a very low cost, making it the optimal tool for this task. In the last years, openly accessible remote sensing data have improved significantly in terms of spatial resolution and return rate. In combination with the recent progress in processing techniques, this has led to significant advances in the assessment and monitoring of aeolian sand dunes worldwide (Hugenholtz et al. 2012; Zheng et al. 2022).

A majority of these dune monitoring approaches are based on optical satellite data. The potential of synthetic aperture radar (SAR) data, however, has not been fully explored as of yet, despite the positive reception in early studies (Blumberg 1998; Qong 2000). The main advantages of SAR over optical imagery are the lack of dependence on atmospheric conditions and lighting and the easy discrimination of

* Corresponding author.
E-mail address: bruno.boemke@geo.rwth-aachen.de (B. Boemke).

https://doi.org/10.1016/j.aeolia.2023.100876
Received 17 November 2022; Received in revised form 21 March 2023; Accepted 25 April 2023
Available online 5 May 2023
1875-9637/© 2023 The Author(s). Published by Elsevier B.V. This is an open access article under the CC BY-NC-ND license (http://creativecommons.org/licenses/by-nc-nd/4.0/).

dunes due to the low volume scattering on sand in most associated microwave frequencies (Nashashibi et al. 2012). Therefore, the analysis and monitoring of single dunes or small aggregations which are easily distinguishable from coarser or vegetated surroundings have been the focus of recent SAR-based studies such as Havivi et al. (2018) and Delgado Blasco et al. (2020). While these studies show promising results in detecting and tracking dune features, they can only be applied where aeolian dunes are surrounded by high-backscatter surfaces. Complex dune fields, however, are much more challenging to analyse, as interdune boundaries show no significance differences in backscatter. The few studies that do access complex dune fields such as Mahmoud et al. (2020) and Manzoni et al. (2021), are using interferometric methodologies or offset tracking. While these methods are well-suited to assess surface stability as well as displacement rates and directions, they only measure relative and absolute changes while neglecting dune morphology. However, as the dune morphology reflects past and present aeolian activity as well as sediment availability, we don't think that this factor should not be omitted in dune field analysis. Therefore, the main aim of this study is to explore the potentials and limitations of SAR imagery for assessing dune morphology in complex aeolian dune fields.

For this, we aim at developing a new method based on Sentinel-1 satellite imagery coupled with the spectral approach of continuous wavelets to assess the morphology of complex dune fields and investigate their temporal and spatial evolution. The new method will be applied and tested on the large Western Mongolian dune field Bor Khyar where the aeolian processes and dune morphology are not thoroughly investigated as of yet.

Materials and methods

The study area

The dune field Bor Khyar Els was selected as the study area due to its complexity in time and space and previous studies by the authors in this region. It is located in the so-called *Valley of the Great Lakes* in Western Mongolia, which consists of several large catchments, ultimately draining into the endorheic lakes Uvs Nuur, Khyargas Nuur and Khar Nuur. Each of these lakes marks the starting point of a large dune field as can be seen in Fig. 1. The large basin has a minimum elevation of 800 m above sea level (asl) in the north and 1200 m asl in the south and is surrounded by the Altai and Khangai mountains, where summits reach more than 4000 m asl. While the central parts of these mountains are made up of Palaeozoic granites and gneiss and the margins by metamorphic and sedimentary rocks (Lehmkuhl 1999), the basin itself is mostly covered by thick layers of fanglomerates, dune sands and lacustrine sediments (Walther and Naumann 1997). Within the basin, landforms such as vast dune fields, widespread alluvial fans and beach ridges up to 130 m above current lake level hint at large climatic variations in the past, which were investigated in numerous studies (Grunert et al. 2000; An et al. 2008; Klinge et al. 2017; Lehmkuhl et al. 2018; Klinge and Sauer 2019).

The recent climate is mainly characterized by extreme continental conditions. As such, temperatures reach less than −20 °C in winter but close to 20 °C in summer. The precipitation in the area has its main gradient between the arid basin, reaching an annual precipitation of 50 mm in some parts, and the semi-arid mountain ranges with an annual precipitation of 200–400 mm (Klinge 2001). Annual precipitations vary

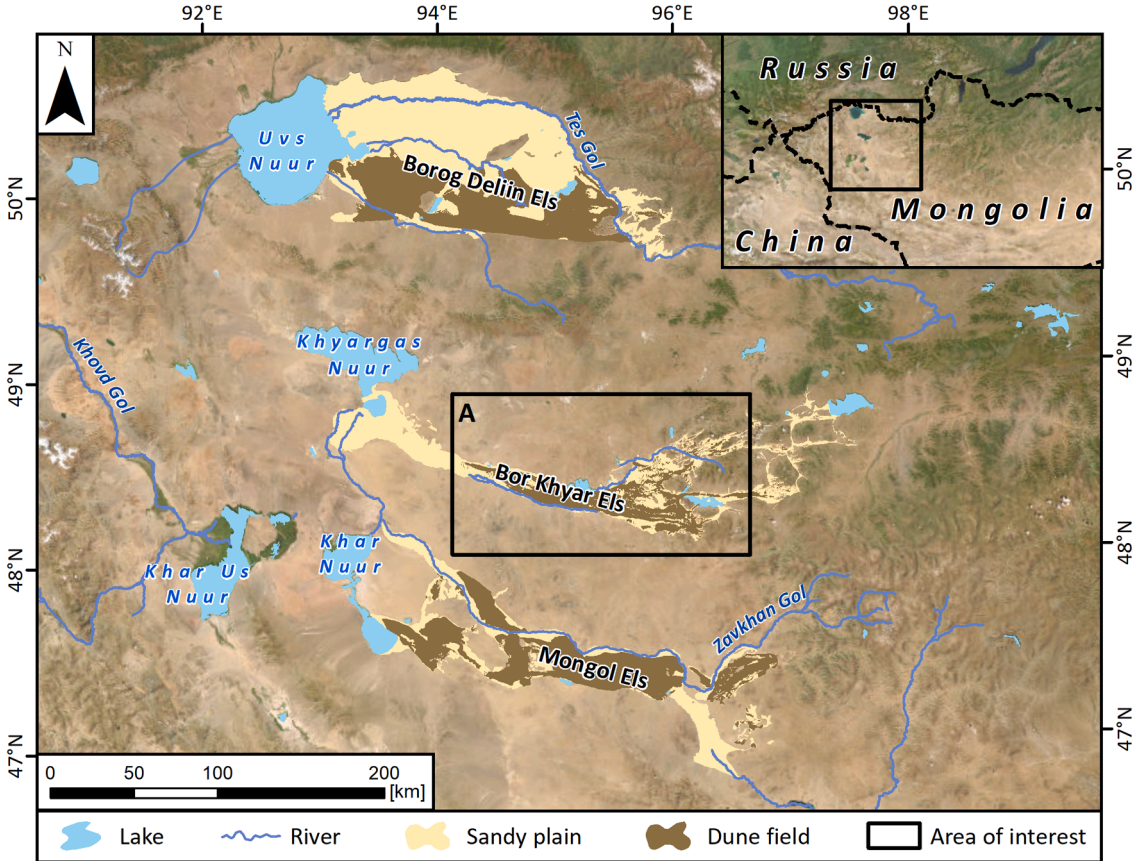

Fig. 1. An overview map showing the valley of the great lakes in western Mongolia. The large dune fields Borog Deliin Els, Bor Khyar Els and Mongol Els are stretching from an endorheic lake in the west into the mountains in the east. The map consists of high resolution satellite imagery (Esri, 2022) which is overlaid by lake, river and dune field signatures.

strongly over the seasons with 70–80% falling during the early summer months (Lehmkuhl and Klinge 2000). The wind regime is mainly influenced by westerly to north-westerly winds, reaching the highest wind speeds in the winter months. In the summer, far weaker winds from the south-east prevail (C3S, 2017).

The Bor Khyar Els dune field itself was formed by westerly winds during the Pleistocene and Holocene and stretches from the Khyargas Nuur lake in the west high into the Khangai mountains in the east (Grunert and Lehmkuhl 2004). It covers a distance of more than 200 km with a maximum width of about 40 km. In its mid-section, the dune field dams off the Bayan Nuur lake, as the westward advance of the water is blocked by vertical offset from a north–south running tectonic fault line (Enkhbold et al., 2022). The two neighbouring dune fields, Borog Deliin Els in the north and Mongol Els in the south, both display a cyclic sand system. This means that sand is transported upslope and westwards through the wind where it is bound by the river system and transported downslope and eastwards again. The Bor Khyar Els, however, lacks a strong adjacent fluvial system that can act as a natural barrier to the aeolian processes and transport sand downslope into the source lake (Grunert and Lehmkuhl 2004). Instead, after traveling 800 m vertically up-slope, the sand disperses into several smaller dune fields situated within mountain valleys.

Preliminary visual analyses of the dune field based on high resolution optical satellite imagery reveal a large variety of dune types and related sandy surfaces including sandy plains, transverse dunes, grid dunes, longitudinal dunes, parabolic dunes as well as barchans. A preliminary analysis of the ERA5 climate dataset reveals large seasonal differences in wind with the strongest winds in winter from west to northwest (C3S, 2017). Based on this preliminary analysis, three areas of interest (AOIs) with differences in complexity, dune types and wind conditions were selected for a detailed analysis. The AOIs include; (A) The Bor Khyar dune field as a whole, (B) A system of dense large transverse dunes, superposed and surrounded by smaller transverse dunes and grid dunes in the south of the dune field, (C) A system of presumably inactive separated large transverse dunes, surrounded by sandy plains in the north of the dune field and (D) A system of transverse and grid dunes in the north-east of the dune field. Fig. 2 offers a first overview over these AOIS as well as ERA5 wind directions and speeds over AOI A.

Sentinel-1 SAR imagery

Although early studies saw great potential in SAR data for the extraction of dune characteristics (Blumberg 1998; Qong 2000), requirements for a continuous global monitoring at high spatial resolution have only been met since the launch of Sentinel-1 in 2014 (Torres et al.

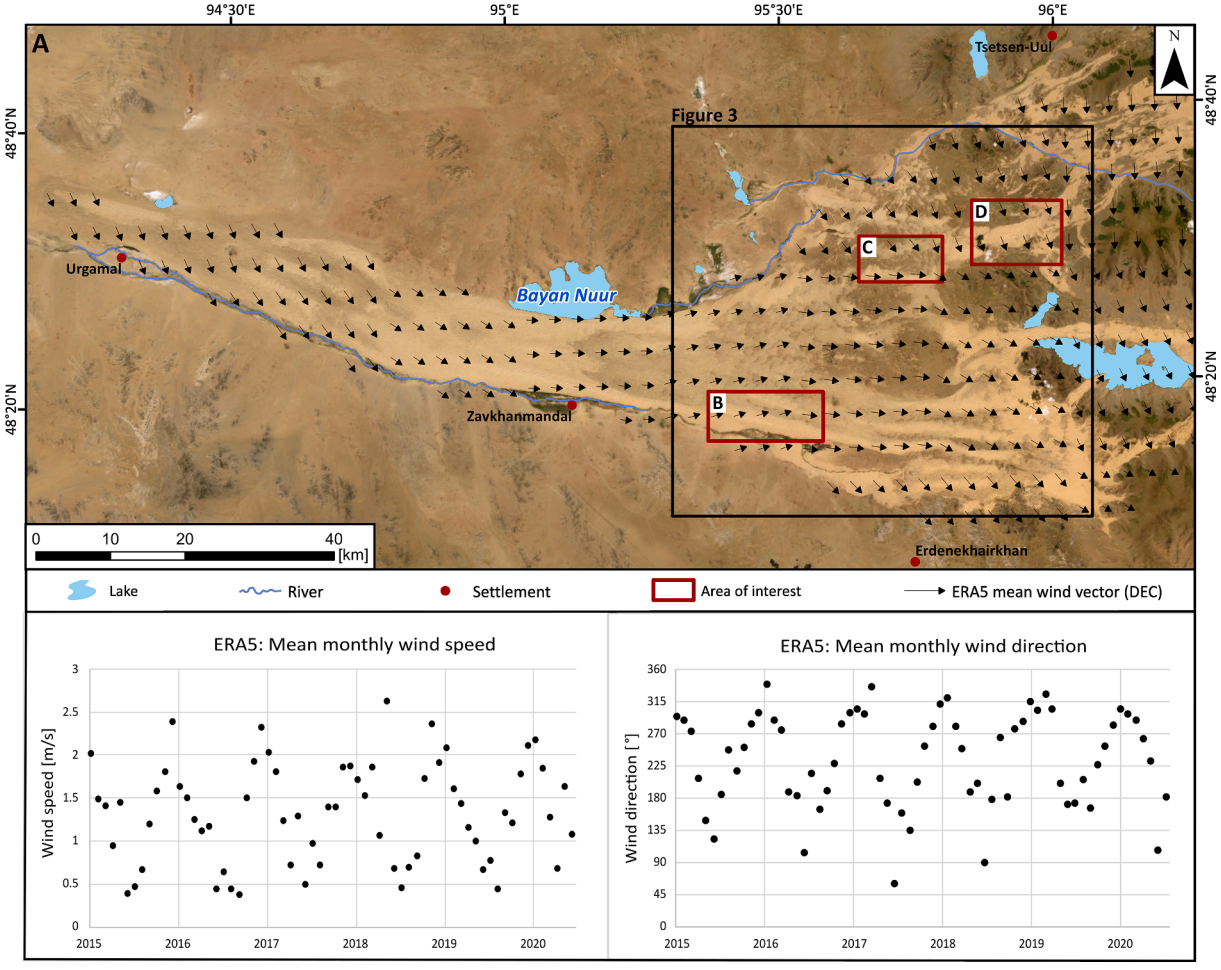

Fig. 2. Upper half: A map of the large dune field Bor Khyar which starts in the west and disperses into the mountains in the east. The map consists of high resolution satellite imagery, clearly showing the dune structures. The imagery is overlaid by wind vector arrows calculated as mean from ERA5 daily data for the month December between 2015 and 2021. The vectors show differing wind directions from northwest, to west, to north (from west to east). Four squares in the east of the map mark the outline of Fig. 3 as well as the areas of interest (AOIs) used in the later study. Lower half: Two scatter point graphs showing ERA5 mean monthly wind speed and direction for the dune field. The main message is that the highest mean wind speeds occur during winter from west to north while lowest wind speeds occur during summer from east to south.

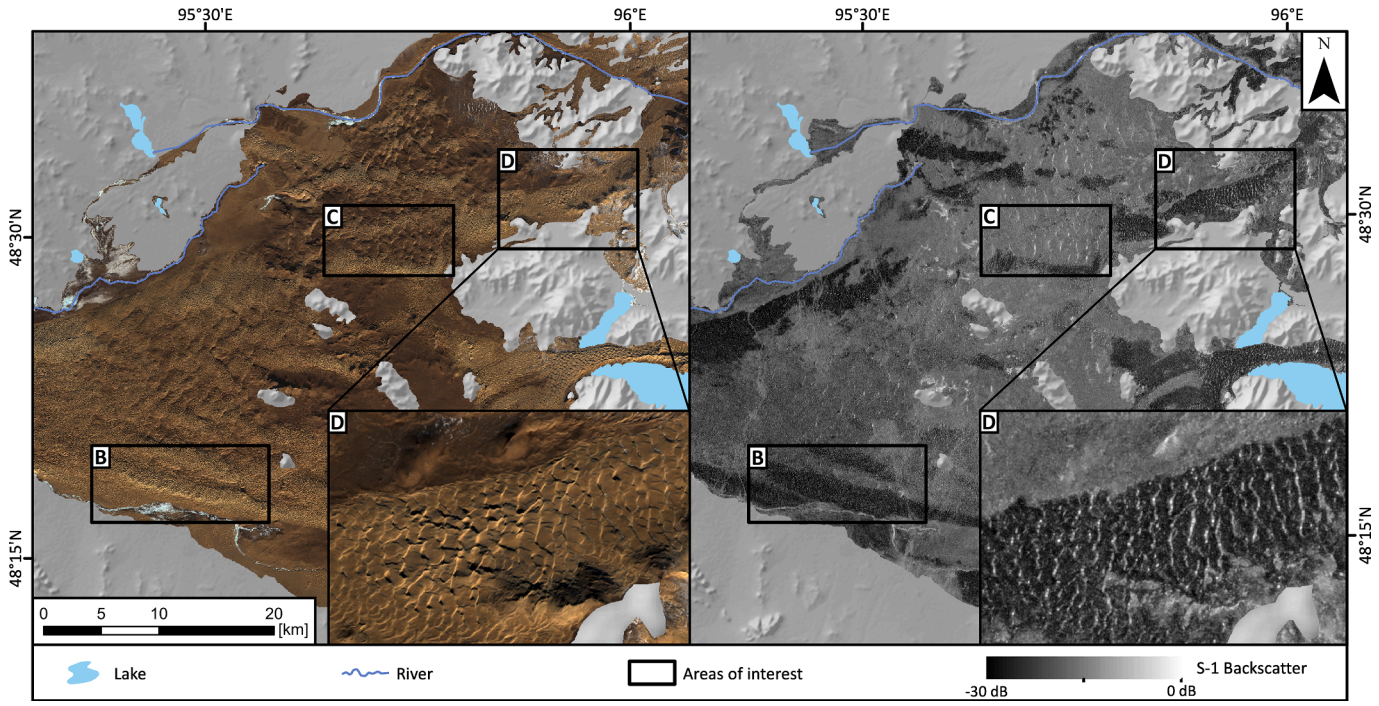

Fig. 3. Two maps showing the eastern part of the dune field, where the dunes disperse into the mountains. The left map shows optical imagery in true colours and the right map shows SAR imagery in greyscales. A zoomed-in cut-out in the lower right offers a closer look. In the background, the non-sandy mountains can be seen as a hillshade. Three rectangles mark the areas that were selected for detailed analysis.

2012). The main advantage that Sentinel-1 has over its predecessors are the high spatial resolution of 10*10 m in the main acquisition mode (Interferometric Wide Swath, IDW), a short repeat cycle of 1–6 days when combining both S-1A and S-1B satellites and the possibility of single and dual polarisations (Geudtner et al. 2014). In combination with the broad availability and easy accessibility, this makes Sentinel-1 the ideal tool for SAR-based assessment as well as continuous monitoring of dunes.

Sentinel-1 operates within the C-Band with a wavelength of 5.6 cm. At this wavelength, even thin layers of sand cannot be penetrated. In combination with the very low backscatter on sand due to the relative surface smoothness, this wavelength allows for a clear differentiation between sand and surrounding surfaces (Williams and Greeley 2004). Within active dunes fields, differences in backscatter can mainly be attributed to the local incidence angle, as the influence of vegetation and grain size differences can be neglected here. As such, slopes that are oriented towards the sensor show slightly elevated backscatter than those that are oriented away from the sensor (Blumberg 1998). With sufficient spatial resolution, this allows for the detection of smaller aeolian forms, superposing the main dune forms. The most prominent dune feature that can be easily extracted with C-band SAR is the ridge, as its morphology leads to double-bounce backscattering (similar to a corner reflector), resulting in a backscatter far higher than the surroundings (Blumberg 1998; Delgado Blasco et al. 2020). These general assumptions towards the SAR-interaction of dunes can be visually confirmed in Fig. 3.

Geospatial processing

As morphological dune parameters can be directly extracted from digital elevation models (DEM), the first attempt was to create a DEM from Sentinel-1 scenes. For this, the workflow for Sentinel-1 based DEM extraction proposed by Braun (2021) was applied to two scenes from the dates 2021–02-10 and 2021–02-22. The main criteria for the identification of these two scenes was the short temporal baseline of 12 days and a large perpendicular baseline distance of 152 m, which were identified using the online baseline tool by the Alaskan Satellite Facility (ASF 2022). The resulting DEM showed promising results for inactive dune fields and the surrounding mountain ranges. Within active dune fields, however, elevations showed large negative deviations and an overall implausible result. This can be attributed to the very low backscatter on sand and the large variation in backscatter within small distances resulting in a very low coherence, which is challenging for interferometric SAR analysis. As such, the DEM-approach was dismissed. Instead, we focused on the indirect derivation of morphological features from Sentinel-1 ground range detected (GRD) data.

The pre-processing and extraction of Sentinel-1 GRD scenes as well as the ERA5 wind analysis was conducted within the Google Earth Engine (GEE), an openly accessible cloud-based platform for geospatial analysis, powered by the Google server infrastructure (Gorelick et al. 2017). For Sentinel-1, we chose to work with the VV-polarized dataset, as it shows the highest dependency on the local incidence angle. To achieve analysis-ready-data (ARD), the pre-processing included additional border noise correction, speckle filtering and radiometric terrain normalization. For this, we used a slightly modified version of the openly accessible ARD script by Mullissa et al. (2021), applying a 10-scene multi-temporal improved Lee sigma speckle filter with a kernel size of 15 cells (Lee et al. 2009). For the terrain normalization, the NASA SRTM global digital elevation model was used (Farr et al. 2007). Based on a preliminary visual interpretation, pre-processed Sentinel-1 scenes from 4 dates were selected and exported for further processing. The dates include 2015–01-31, 2018–06-14, 2018–10-12 and 2021–12-07, each for which a Sentinel-1 GRD mosaic of the whole dune field was created. The GEE was also used to calculate wind direction and speed from ERA5 wind u-component and v-component. Monthly data was used to aggregate speed and direction over the full timespan (2015–2021) while wind vectors for visualization were created from daily data.

For the indirect derivation of morphological features as well as an analysis of their evolution in time, a frequency analysis in form of the continuous wavelet transform (CWT) was applied to these mosaics. To

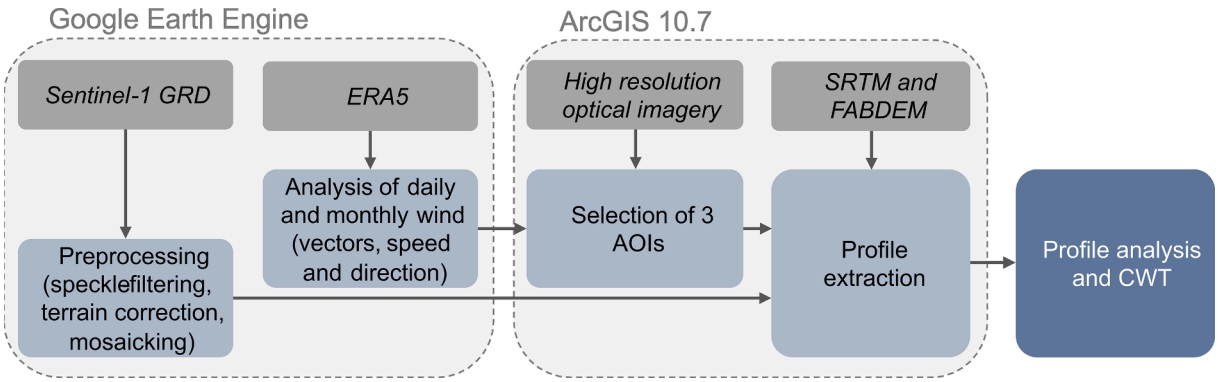

Fig. 4. Workflow diagram showing the different processing steps and the environments they were conducted in. Datasets are displayed in grey, processing steps are displayed in light blue and the central part of the study, the profile analysis and continuous wavelet transform (CWT) are displayed in dark blue. The workflow starts on the left, where Sentinel-1 and ERA5 are preprocessed and analysed in the Google Earth engine. It then focusses on the creation of 3 areas of interest which are then used to extract profiles based on Sentinel-1 and DEM data. The resulting profiles are then used for profile analysis and continuous wavelet transform. (For interpretation of the references to colour in this figure legend, the reader is referred to the web version of this article.)

compare these backscatter values to a directly derived morphology, SRTM and FABDEM elevation model profiles were also extracted (Farr et al. 2007; Hawker et al. 2022). Both elevation models have a spatial resolution of 25*25 m in the study area. While the SRTM represents a surface from the year 2000, the FABDEM is an improved version of the Copernicus GLO-30 DEM that was surveyed between 2011 and 2015. As such, the comparison between the two DEMs offers a first assessment of dune activity. For the profile extraction, the already mentioned AOIS were used, representing different dune types and different levels of complexity (see Figs. 2 and 3). For the spatial processing and extraction of profiles, we used ArcGIS, version 10.7.1. The pre-processing for profile analysis included reprojection into a metric coordinate reference system (WGS84, UTM Zone 46 N, EPSG:32646) and resampling into the same spatial resolution of 10*10 m. In each AOI, a central tracking axes was defined manually, representing the centreline of the local dune field along the wind direction. Four additional profiles parallel to each central tracking axis were extracted in distances of 200 and 400 m left and right. The resulting lines were used to extract S-1 and SRTM surfaces to profiles. These profiles were then extracted as csv text files via the 3D Analyst toolbar, ready for the visualization in Excel 2016 and the CWT analysis. To enhance the understanding of this multi-step workflow, it is visualized in Fig. 4.

Spectral analysis based on wavelet transform for the morphological decomposition

From a technical point of view, dune fields, such as the ones investigated in this research, can be seen as a set of spatially variable morphological features at different scales. This association gets clear when looking at the profiles portrayed the Figs. 5, 6 and 7. The spacing and size of these features is a function of wind interactions with a surface and sand availability. The variability of such dunes in response to external forces such as wind follows a non-linear pattern. All changes result in a combination of several morphological modulations at various ranges of spatial scales. Therefore, we used an approach to investigate the spatial frequencies of morphological changes by decomposing the total variability to a series of scales. This method is useful to identify the evolution of dunes and their organization in response to the external drivers of aeolian energy and internal drivers associated to the characteristics (texture, age, …) of sediments composing these morphological forms.

To do so, we used the techniques of Continuous Wavelet Transform (CWT), which are well documented in Labat et al. (2005) works and well-known for hydrological, meteorological and climate applications (e.g. Turki et al. 2015; Massei et al. 2017). The CWT has been explored by Turki et al. (2021) for other applications related to the morphology of intertidal dunes and their migration under the wave-tide interactions, case of the Baie de Somme (France). These publications have demonstrated the relevance of this method to gain more insights into the evolution of morphological structures at different temporal and spatial scales.

When applying a CWT analysis, a complex signal (e.g. Sentinel-1 profiles through dune fields) is scanned using different wavelengths. While scanning with a wavelength, high rhythmicity results in a high power of this wavelength, while absent rhythmicity is reflected by low power. This way, the rhythmicity and thereby relevance of each tested wavelength is collected along the signal/profile. The resulting CWT-Diagram gives a good overview of which wavelengths of dune features are relevant along the profile. Spatial and temporal differences in the CWT diagram allow an interpretation of the morphological forces. Taking advantage of this approach, changes in dune features, detected via Sentinel-1 SAR imagery, as well as the possible rhythmic structures of dunes associated to the sediment transport dynamics and the aeolian activity were explored.

The CWT has been carried out for the four Sentinel-1 scenes mentioned in the *geospatial processing* at different profiles along the AOIs B, C and D. For the assessment of cross-axis variability, the CWT was applied to each central axis as well as four parallel axes 200 and 400 m north and south of the central axis (see Figs. 5, 6 and 7 for localization of the central axes).

Table 1
Short description of the different areas of interest (AOIs) and which methods were applied in them.

AOI	Description	Visual interpretation	Profile analysis	CWT
A	The Bor Khyar dune field as a whole	+	–	–
B	A system of dense large transverse dunes, superposed and surrounded by smaller transverse dunes and grid dunes	+	+	+
C	A system of presumably inactive separated large transverse dunes, surrounded by sandy plains in the north of the dune field	+	+	+
D	A system of transverse and grid dunes in the north-east of the dune field	+	+	+

The CWT diagrams contain: (1) the contour diagram with space along the profile in meters*10 on the x-axis; (2) the wavelength of morphological features (dunes) in meters*10 on the y-axis; and (3) the power or variance on the z-axis.

Results

In the following section, the Sentinel-1 images are visually interpreted in comparison to optical imagery and a DEM. In addition, the extracted profiles along the central tracking axes are presented and analysed. In the second part of the results we then present the results of the CWT frequency analysis. Table 1 gives an overview over which methods were applied in the different AOIs.

Visual interpretation and profile analysis

In the visual interpretation of the whole dune field (**AOI A**), Sentinel-1 scenes, Sentinel-2 true colour composites and the SRTM DEM were compared. This comparison confirms the expectations about the C-Band sensitive backscatter characteristics of active and inactive dunes, stated in the *materials and methods*. As such, it could be observed that active dune fields can be separated from inactive dune fields and surrounding areas by their lower backscatter.

For a simple thresholding approach, a backscatter of < -20 dB yielded the best results in differentiating active dunes across all scenes. The only other surfaces in the study area that fall below this threshold are lakes. Confusion between these two surface types, however, can be easily avoided by the complementary use of optical imagery and/or surface water datasets.

The only features within active dune fields, that do not fall below the

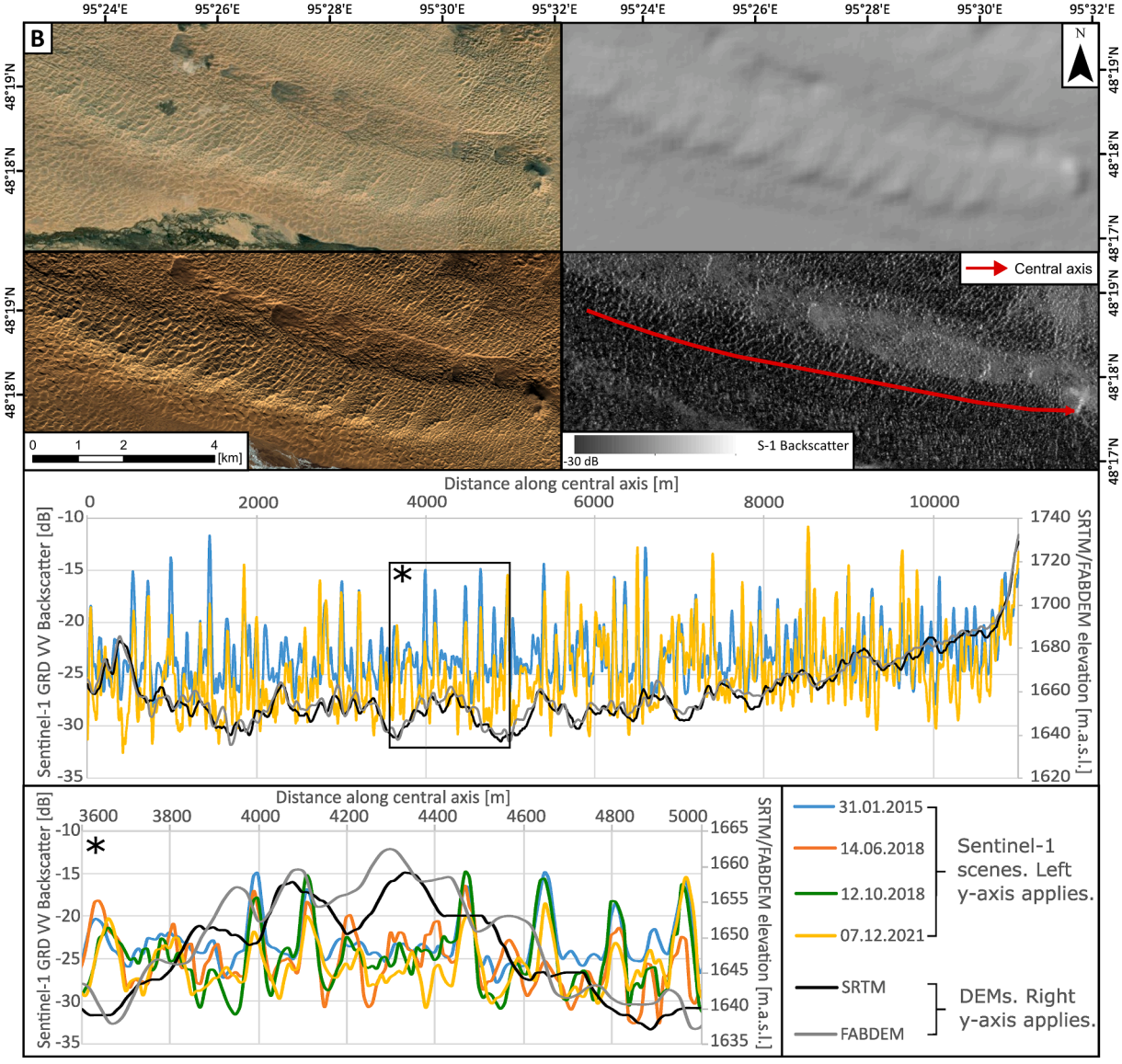

Fig. 5. On the top half, four maps are depicted, showing a comparison of close-up maps of AOI B. This includes high resolution optical imagery (upper left), the SRTM DEM in greyscales (upper right), Sentinel-2 optical imagery in true colours (lower left) and Sentinel-1 GRD SAR imagery in greyscales (lower right). The dune can be clearly seen as a west-north-west to east running elongated elevated chain of ridges with smaller ripples in between. On the SAR imagery, a red line represents the central axis. On the lower half of the figure, the Sentinel-1 backscatter profiles from the different scenes (2015–2021) as well as SRTM and FABDEM elevation along the tracking axis are displayed. While the profiles as a whole seem to be a chaotic sequence of peaks and valleys, the close up at the bottom shows a clearer picture: The highest SAR backscatter peaks migrate downwind while the smaller peaks and valleys in between vary strongly. This indicates active conditions, which is supported by the changes in the DEM. (For interpretation of the references to colour in this figure legend, the reader is referred to the web version of this article.)

threshold, are dune ridges. Instead, they show strongly elevated backscatter values, reaching above 0 dB at bend points within dune slip surfaces (see Fig. 3 and/or Fig. 7). This supports the double-bounce backscatter interaction and corner-reflector-similarity mentioned in the materials and methods. A direct comparison to optical imagery shows the importance of the direction of illumination: ridges perpendicular to the illumination direction are enhanced while ridges parallel to the illumination direction only show slightly elevated backscatter or no difference in backscatter at all (see Fig. 3 and/or Fig. 7).

Within the south-western **AOI B**, the visual interpretation of SAR, optical imagery and the DEMs in comparison show the main limitations of Sentinel-1-based complex dune field analysis. As can be seen in Fig. 5, the Sentinel-1 scene still allows for an easy differentiation between inactive and active dune fields as well as an easy identification of dune ridges perpendicular to the illumination direction. This information, however, can only be obtained for the superposing grid-dune structures with inter-ridge-distances of about 100–200 m. The underlying large transverse forms with wavelengths of about 1000 m, which can be clearly seen in both the optical imagery as well as the DEMs, are not visible in the Sentinel-1 scenes.

In the Sentinel-1 profile graphs, no differences in backscatter between the underlying large transverse dune slope facing the sensor and facing away from the sensor can be detected, either. As such, only information about the superposing grid dunes can be extracted from these profiles. In comparison to the DEM profiles, showing only the underlying transverse forms and 2–4 superposing grid dune ridges on each of these, the Sentinel-1 profiles provide surface information in far higher detail, including several peaks and valleys in between the main superposing grid dune ridges. These changes in backscatter between ridges are most probably triggered by differences in the local incidence angle, indicating ripple features. When comparing the Sentinel-1 profiles from different dates, the highest peaks, indicating main dune ridges, show a high overlap. However, the magnitude of the peaks differs widely between the scenes, showing differences of up to 15 dB. In addition, a shift of several meters along the profile axis through time can be observed in many cases, indicating wind-induced dune movement and as such active aeolian conditions. This is additionally supported by the differences between the SRTM and FABDEM elevation, showing a windward dune

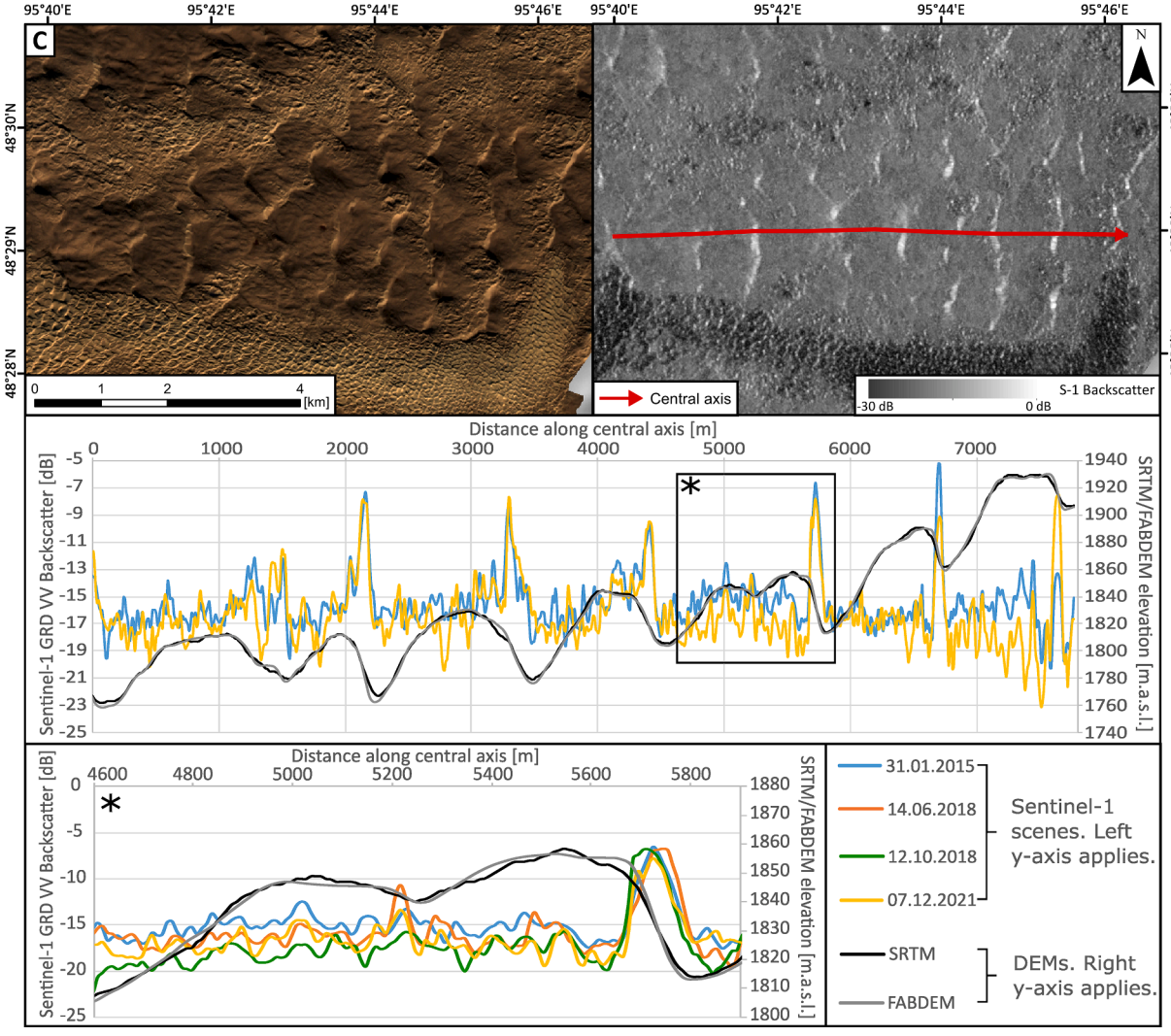

Fig. 6. On the top half, two maps are depicted, showing a comparison of close-up maps of AOI C. This includes Sentinel-2 optical imagery in true colours (left) and Sentinel-1 GRD SAR imagery in greyscales (right). The dune can be recognized stretching from west to east through a chain of long ridges with vast spaces in between. On the SAR imagery, a red line represents the central axis. On the lower half of the figure, the Sentinel-1 backscatter profiles from the different scenes (2015–2021) as well as SRTM and FABDEM elevation along the tracking axis are displayed. While the profiles as a whole seem to be a chaotic sequence of peaks and valleys, the close ups at the bottom show a clearer picture: The highest SAR backscatter peaks are located at the DEM ridges and no clear direction of dune migration can be seen. The inter-ridge variations are also comparatively low and the DEMs show a very high alignment. This indicates inactive conditions. (For interpretation of the references to colour in this figure legend, the reader is referred to the web version of this article.)

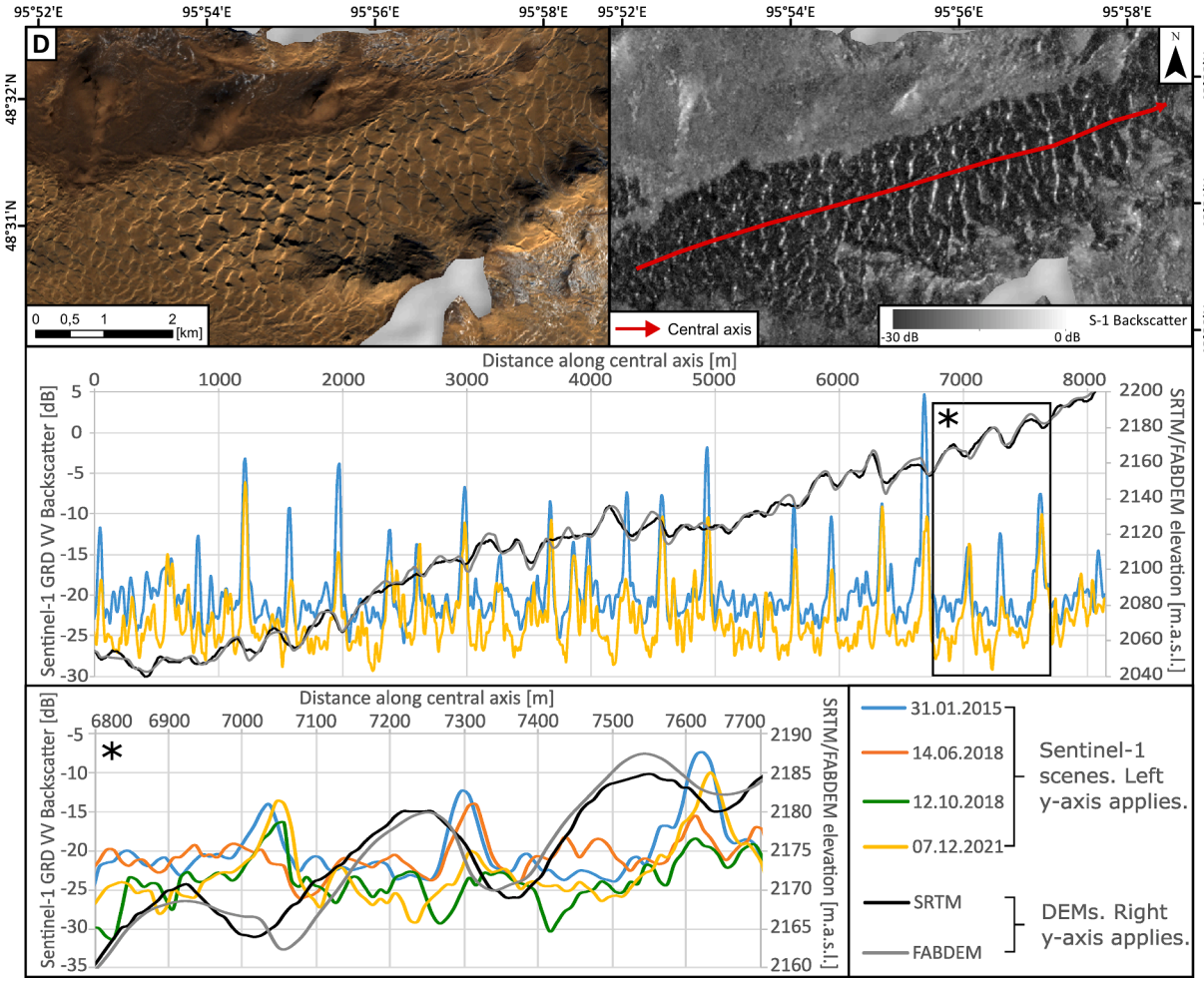

Fig. 7. On the top half, two maps are depicted, showing a comparison of close-up maps of AOI D. This includes Sentinel-2 optical imagery in true colours (left) and Sentinel-1 GRD SAR imagery in greyscales (right). The dune can be clearly seen as a west-south-west to east-north-east running elongated chain of long ridges. On the SAR imagery, a red line represents the central axis. On the lower half of the figure, the Sentinel-1 backscatter profiles from the different scenes (2015–2021) as well as SRTM and FABDEM elevation along the tracking axis are displayed. While the profiles as a whole seem to be a chaotic sequence of peaks and valleys, the close ups at the bottom show a clearer picture: The highest SAR backscatter peaks are located at DEM dune ridges and migrate downwind while the smaller peaks and valleys in between vary strongly between each date. This indicates active conditions, which is supported by the changes in the DEM. (For interpretation of the references to colour in this figure legend, the reader is referred to the web version of this article.)

migration between the years 2000 and 2011–2015.

The northern **AOI C** shows large visual differences in comparison to the other AOIs. The main ridges show far higher distances of 700 to 1100 m. In the Sentinel-1 scenes, only slight variations in backscatter can be observed between these main ridges. In addition to that, the backscatter is generally higher, not falling under the threshold for finely grained active dune sand of −20 dB. The comparison between the SRTM and FABDEM also show a high overlap. Within the optical Sentinel-2 imagery, no indications for vegetation can be found in these areas. As such, the higher backscatter is most likely caused by larger grain sizes, indicating inactive conditions where the finely grained sand is eroded.

In the Sentinel-1 profile graphs of AOI C, the overlap of peaks and valleys along the profile axis is the highest among all AOIs. This supports the assumption of inactivity based on the visual interpretation. When assuming temporal stability, this part of the dune field offers the opportunity to locate the double-bounce-related high backscatter in the Sentinel-1 profiles in comparison to the FABDEM morphology. As Fig. 6 shows, this peak is located at the steepest part of the slip face, supporting the double-bounce assumption. Therefore, when trying to extract ridges via Sentinel-1, a certain offset between the highest backscatter and the actual ridge has to be considered.

The north-eastern **AOI D** shows a complex system of transverse, grid and barchanoid dunes. The mean inter-ridge-distance is between 200 and 300 m, showing a high variability within the AOI. Within both the optical and the SAR imagery, differences within the AOI, especially between the northern and southern part, can be observed. While most dunes in the south seem to be formed by westerly winds as indicated by their north to south-alignment, dunes in the northern parts of the AOI shift towards a north-east to south-west alignment, indicating stronger north-westerly winds. This fits the ERA5 wind data, showing the strongest winds from north-west during winter in this part of the dune field (see Fig. 2). Due to the importance of the illumination direction, some dune ridges showing the strongest east-to-west alignment are not represented in the Sentinel-1 GRD imagery (see Fig. 7).

The central tracking axis profile graphs of AOI D show many similarities to AOI B. Comparing the different Sentinel-1 scenes, the main ridges show a high overlap with a slight shift along the tracking axis through time, indicating wind-induced dune movement. A far higher variability can be seen in between the main ridges, indicating vast changes in superposing sand forms such as ripples. These assumptions towards aeolian activity are additionally supported by the comparison between the SRTM and FABDEM, showing windward dune migration.

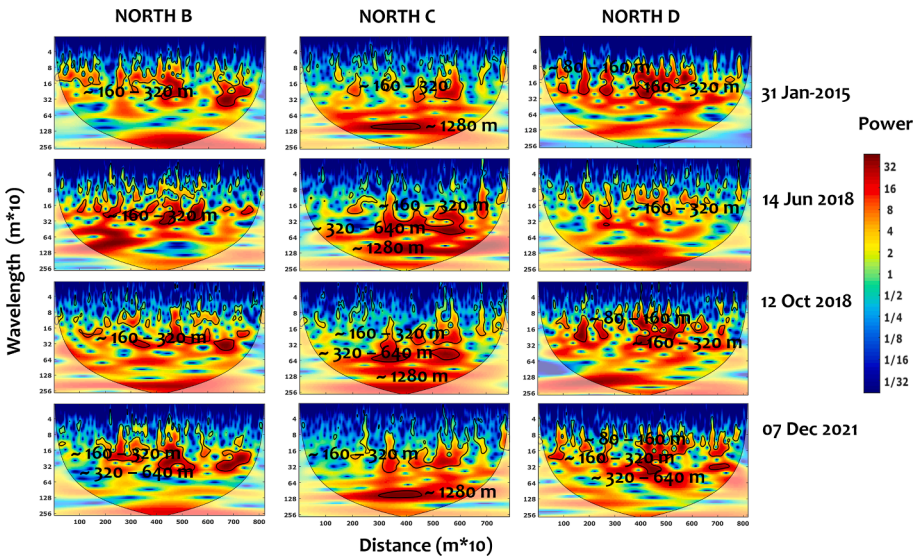

Fig. 8. The figure shows 12 *Continuous wavelet transform (CWT)* diagrams of the NORTHERN profile axes of all Sentinel-1 scenes in each AOI. The timescale can be seen as running from the top (January 2015) to the bottom of the figure (December 2021). Each diagram shows the power of variance (colour-coded from blue/weak to red/strong) of morphological structures at different wavelengths (y-axis, unit: m*10) and at different positions along the AOI (x-axis, unit: m*10). Significant variances can be seen in the wavelengths from 8 to 128 m*10 but they vary strongly between the AOIs. AOI D shows the shortest significant wavelength and AOI C the longest. The detailed interpretation of the diagrams is explained in the following text. (For interpretation of the references to colour in this figure legend, the reader is referred to the web version of this article.)

Continuous wavelet transform

The spectral approach of continuous wavelet transform (CWT) has been used comparatively in the AOI's B, C and D to investigate the present morphological forms as well as their inter-annual and intra-annual variability with the aim to identify the morphological modulations of dunes. Based on absolute and relative differences between these modulations, the aeolian activity and its influence on the dune changes are discussed. In this section, we are presenting the results for three cross sections of each AOI, namely north (Fig. 8), central (Fig. 9) and south (Fig. 10), represented by the central tracking axis and the parallels in 200 m distance. This approach is useful to identify the different rhythmic patterns controlling the dune variation (erosional vs depositional areas) and the wavelength of the associated morphological forms. The application of the CWT to the different AOI's sections has highlighted the presence of dune modulations and their associated morphological dune features as well as their evolution through time.

As can be seen in Figs. 8–10, the distribution of energy in the CWT spectrum is non-uniform with altering bands of high and low power, represented by red and blue colours, respectively. This distribution highlights the existence of several modulations of morphological changes structured at a series of spatial periods with different wavelengths, divided into the categories ~ 8–16 (shortest wavelengths, highest spatial frequencies), ~160–320, ~320-640and ~ 1280 m (longest wavelengths, lowest spatial frequencies).

The high power of the ~ 1280 m wavelength seems to be similarly manifested during all years in AOI C at all profiles from the north to the south. Such modulations are associated with the large and inactive dunes in this AOI. The small dune features, shown by the wavelength of ~ 8–16 m*10, are often connected to larger structures (~160–320 and ~ 320–640 m) as illustrated in AOI B and D. This connection seems to be significantly manifested in the north of the AOIs with regular structures, however, it is relatively limited in the centre and the south.

The smaller morphological modulations of ~ 80–160 m exhibit non-organized forms according to the scale range; most of them are observed from the centre to the south of AOI B and vanish in the north of the AOI where the morphological modulations are well structured and strongly connected.

According to the spectral analysis of the morphological dune changes, a series of findings can be formulated as follows:

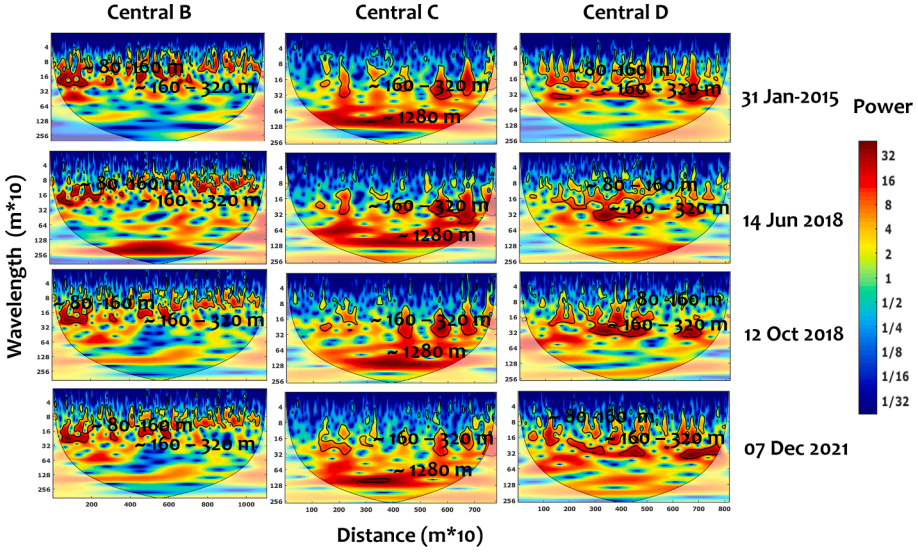

Fig. 9. The figure shows 12 *Continuous wavelet transform (CWT)* diagrams of the CENTRAL profile axes of all Sentinel-1 scenes in each AOI. The timescale can be seen as running from the top (January 2015) to the bottom of the figure (December 2021). Each diagram shows the power of variance (colour-coded from blue/weak to red/strong) of morphological structures at different wavelengths (y-axis, unit: m*10) and at different positions along the AOI (x-axis, unit: m*10). Significant variances can be seen in the wavelengths from 8 to 128 m*10 but they vary strongly between the AOIs. Here, AOI B shows the shortest significant wavelength and AOI C the longest. The detailed interpretation of the diagrams is explained in the following text. (For interpretation of the references to colour in this figure legend, the reader is referred to the web version of this article.)

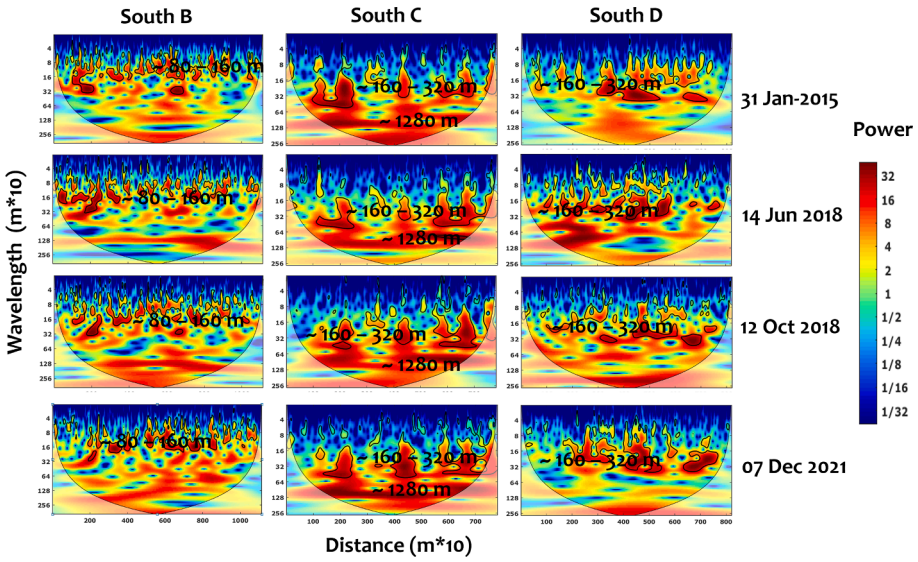

Fig. 10. The figure shows 12 *Continuous wavelet transform (CWT)* diagrams of the SOUTHERN profile axes of all Sentinel-1 scenes in each AOI. The timescale can be seen as running from the top (January 2015) to the bottom of the figure (December 2021). Each diagram shows the power of variance (colour-coded from blue/weak to red/strong) of morphological structures at different wavelengths (y-axis, unit: m*10) and at different positions along the AOI (x-axis, unit: m*10). Significant variances can be seen in the wavelengths from 8 to 128 m*10 but they vary strongly between the AOIs. Here, AOI B and AOI D show similarly short significant wavelengths and AOI C the longest. The detailed interpretation of the diagrams is explained in the following text. (For interpretation of the references to colour in this figure legend, the reader is referred to the web version of this article.)

1. The temporal variation of dune morphology is highlighted by an inter-annual evolution of morphological modulations from 2015 to 2018 which is significantly manifested in AOI D where the dynamics are highly active. This dynamic seems to be extremely reduced for dunes of AOI C.
2. The seasonal patterns of dune changes, reflected from the comparison of dune fields between June and October of 2018, are manifested in the different AOIs and exhibit a pronounced sedimentary connection in winter periods when the sediment transport induced by the increasing aeolian energy is important. However, this connection seems to be reduced during summer periods, most probably due to the seasonal shift in the wind regime (see Fig. 2).
3. The morphological forms of dunes are strongly related to the energetic conditions of wind. The distribution of morphological forms from homogenous structures in AOI B and AOI D (clear connection between small and large dune features) to non-homogenous ones in AOI C (inactive paleo-dunes with limited connections to small dune features) where the sediment transport induced by wind regime seems to be controlled by different directions.

Discussion

Limitations and sources for errors

In comparison to optical imagery, Sentinel-1 GRD data requires an extensive pre-processing procedure before it is in an analysis-ready state. The aim of this procedure is to remove any noise in form of radar speckle, terrain effects and border noise. When applying a speckle filter, however, there is a chance that not only noise is removed but also a part of the signal is smoothed out. The choice of the filtering algorithm and parameters should therefore be considered with caution. Based on this study, we recommend the use of the improved sigma filter (Lee et al. 2009), effectively filtering speckle while preserving the signal. As applying this filter to larger scenes requires a lot of processing power, we additionally recommend the ARD-implementation into the GEE by Mullissa et al. (2021).

Due to the areal low coherence between Sentinel-1 scenes of active dune fields, interferometric approaches and DEM-derivation are not applicable. Therefore, dune morphology and dune features have to be extracted indirectly from GRD scenes. Backscatter differences in active dune fields are mainly influenced by the local incidence angle. Therefore, the direction of dune features in comparison to the illumination direction is one of the main limitations. As could be seen in AOI B, another main limitation is the fact that subsurface forms like the underlying large transverse dunes cannot be detected in GRD imagery. Therefore, it is necessary to include optical imagery or DEMs to assess the dune field comprehensively.

The Sentinel-1 GRD profile analysis in this study has shown that while the backscatter values of the scenes show a high spatial overlap, the absolute backscatter values vary widely between them. For automated thresholding and feature extraction processes, this means that a variable approach has to be applied, evaluating each scene separately.

Potentials and perspective

From Sentinel-1 GRD imagery, three main features relevant for complex dune field dynamics can be extracted. The first is finely grained active dune sand, which can be easily differentiated from coarsely grained or vegetated inactive dunes as well as other adjacent surfaces by its very low backscatter of lower than −20 dB. The second feature is dune ridges, which have a far higher backscatter than the surrounding dune sand due to the double-bounce backscatter effect. This effect, however, is highly dependent on the illumination direction and the curvature and slope of the ridge, leading to large differences in backscatter between scenes. The third type of dune features that can be extracted via Sentinel-1 GRD imagery are smaller scale ripples between the main ridges.

As we have shown in this study, the CWT frequency is a fitting method to analyse these indirectly derived dune features. As such, it provides useful information related to the changes in spatial and temporal morphological modulations of dunes in response to aeolian energy conditions. This approach has given new insights related to the morphological modulations of dunes in time and space. A series of hypotheses have been highlighted; (i) strongest aeolian activity is found in the north of the AOIs which are mainly controlled by an exposure to north-westerly winds, (ii) multi-timescale evolution of dunes can be observed in AOI B and D in response to active aeolian conditions from seasonal to inter-annual scales, while they are weakly active to inactive in AOI C, (iii) strong morphological connections between small and large dune features can be observed during winter periods while these connections are weakly manifested during summer periods when changes in the energy and the direction of wind are significant. As such, this technique has given some insights into the external (climate conditions) and internal (sediment characteristics) drivers controlling the morphological migration of dunes.

The main advantage of Sentinel-1 SAR GRD over optical imagery for

complex dune field analysis is the easy identification of the mentioned morphological features as well as the easy discrimination of inactive and active dunes. This is due to the fact that these different surfaces and features show very little differences in their spectral reflectance, making them difficult to distinguish in optical imagery. In C-band SAR, however, the backscatter is mainly influenced by surface roughness and local incidence angle, allowing an easy differentiation.

The main advantage of Sentinel-1 SAR GRD over openly accessible global DEMs is the higher spatial resolution and multi-temporality. Although the dune morphology could be directly extracted from the SRTM DEM in this study, it lacked the spatial resolution to take smaller forms into account. Due to the possibility of direct extraction of dune morphology, the first attempt in this study was to create a DEM from Sentinel-1 SLC imagery. Due to very low coherence, however, this was not possible in the active parts of the dune field. Instead, the dune morphology was extracted indirectly from GRD imagery. Although this methodology brings some challenges in the analysis and interpretation, the multi-temporality was favoured over the direct dune form extraction.

As the advantages of complex dune field analysis with Sentinel-1 GRD are mainly the easy differentiation of the mentioned features and high spatial and temporal resolution, we see its main value in the automated derivation of dune features. For example, the continuous automated derivation of dune ridges and active dune sand in combination with wind datasets could bring new results for the annual variability of dune movement and the response to storm events.

Conclusion

In this study, we have shown the possibilities as well as limitations in using the currently most easily accessible SAR dataset, Sentinel-1 GRD, to access the morphology of a complex dune field and changes therein. As the very low areal coherence within active complex dune fields does not allow for interferometric approaches such as the calculation of a DEM, we used the GRD backscatter values to extract morphological features indirectly. Using this method, three main dune features can be extracted based on surface roughness and local incidence angle. These are namely active dune sand, dune ridges and inter-dune ripples.

Based on this information, a comparative analysis to optical Sentinel-2 imagery and the SRTM DEM as well as a profile-based continuous wavelet transform frequency analysis were conducted for the complex dune field Bor Khyar Els in western Mongolia. Using these methodologies, three areas of interest within the dune field were analysed, revealing significant differences in aeolian activity, wind direction and wind seasonality.

Based on the results of this study, we see a good suitability of Sentinel-1 for complex dune field analysis. This suitability is additionally amplified by the comparison to similar approaches based on optical imagery and DEMs. In comparison to these datasets, Sentinel-1 allows for a far better detection of dune-relevant morphological features. In comparison to optical imagery where these features only show slight differences in their reflectivity, SAR-based analysis offers an easy discrimination. The main advantage over globally available DEMs is the comparably high spatial resolution and especially the multi-temporality.

Due to these advantages of SAR-based complex dune field analysis, we see great potential in its further implementation. For future studies, we recommend its implementation in automated analyses of continuous time series. Due to the high temporal resolution of Sentinel-1, this would offer new insights into the temporal and spatial evolution of dune fields as well as the related frequencies and magnitudes of the aeolian driving forces.

CRediT authorship contribution statement

Bruno Boemke: Writing – original draft, Writing – review & editing, Investigation, Methodology, Software, Formal analysis, Visualization, Data curation. **Imen Turki:** Writing – original draft, Writing – review & editing, Conceptualization, Methodology, Visualization. **Catrina Brüll:** Conceptualization, Supervision, Funding acquisition. **Frank Lehmkuhl:** Conceptualization, Writing – review & editing, Supervision, Funding acquisition.

Declaration of Competing Interest

The authors declare that they have no known competing financial interests or personal relationships that could have appeared to influence the work reported in this paper.

Data availability

Data will be made available on request.

Acknowledgement

This work was carried out in the frame of the exploratory research space (ERS), funded by the Federal Ministry of Education and Research (BMBF) and the Ministry of Culture and Science of the German State of North Rhine-Westphalia (MKW) under the Excellence Strategy of the Federal Government and the Länder [project ID G:(DE-82)EXS-SF-OPSF612]. We thank Alexandra Weber for the valuable help in reviewing the figures and structure, Damian Stawinoga for testing the interferometric approach and Martha Wingen for the conceptual and administrative help. We would also like to thank the reviewers for the time and effort invested into reviewing the manuscript. Their comments and suggestions helped in improving the quality of the manuscript significantly.

References

Al-Ghamdi, K., Hermas, E., 2015. Assessment of dune migration hazards against landuse northwest Al-lith City, Saudi Arabia, using multi-temporal satellite imagery. Arab J Geosci 8 (12), 11007–11018. https://doi.org/10.1007/s12517-015-1947-8.

Amin, A., Seif, E.-S.-S.-A., 2019. Environmental Hazards of Sand Dunes, South Jeddah, Saudi Arabia: An Assessment and Mitigation Geotechnical Study. Earth Syst Environ 3 (2), 173–188. https://doi.org/10.1007/s41748-019-00100-5.

An, C.-B., Chen, F.-H., Barton, L., 2008. Holocene environmental changes in Mongolia: A review. Global and Planetary Change 63 (4), 283–289. https://doi.org/10.1016/j.gloplacha.2008.03.007.

Asf Alaskan Satellite Facility baseline tool. Available online at https://baseline.asf.alaska.edu 2022 updated on 5/3/2022.

Benjaminsen, T.A., Hiernaux, P., 2019. From Desiccation to Global Climate Change: A History of the Desertification Narrative in the West African Sahel, 1900–2018. Global Environment 12 (1), 206–236. https://doi.org/10.3197/ge.2019.120109.

Blumberg, D.G., 1998. Remote Sensing of Desert Dune Forms by Polarimetric Synthetic Aperture Radar (SAR). Remote Sensing of Environment 65 (2), 204–216. https://doi.org/10.1016/S0034-4257(98)00028-5.

Braun, A., 2021. Retrieval of digital elevation models from Sentinel-1 radar data – open applications, techniques, and limitations. Available online at Open Geosciences 13 (1), 532–569. https://doi.org/10.1515/geo-2020-0246.

C3S, 2017. ERA5: Fifth generation of ECMWF atmospheric reanalyses of the global climate. Copernicus Climate Change Service Climate Data Store (CDS), https://cds.climate.copernicus.eu/cdsapp#!/home (last visited May 3, 2023).

Davies, J., Ogali, C., Laban, P., Metternicht, G., 2015. Homing in on the range: enabling investments for sustainable land management. In *Technical brief* (29.01.2015), IUCN and CEM. Available online at.

Delgado Blasco, J.M., Chini, M., Verstraeten, G., Hanssen, R.F., 2020. Sand Dune Dynamics Exploiting a Fully Automatic Method Using Satellite SAR Data. Remote Sensing 12 (23), 3993. https://doi.org/10.3390/rs12233993.

El Gammal, E.S.A., El Gammal, A.E.D.A., 2010. Hazard impact and genetic development of sand dunes west of Samalut, Egypt. The Egyptian Journal of Remote Sensing and Space Science 13 (2), 137–151. https://doi.org/10.1016/j.ejrs.2010.02.001.

Eljack, E., Csaplovics, E., Adam, H., 2010. Mapping and assessment of sand encroachment on the Nile River northern Sudan, by means of remote Sensing and GIS. Available online at. https://citeseerx.ist.psu.edu/viewdoc/download?doi=10.1.1.1065.4&rep=rep1&type=pdf.

Enkhbold, A., Khukhuudei, U., Kusky, T., Tsermaa, B., Doljin, D., 2022. Depression morphology of Bayan Lake, Zavkhan province, Western Mongolia: implications for the origin of lake depression in Mongolia. Phys. Geogr. 43 (6), 727–752.

Esri, 2022. "Imagery" [basemap]. At different scales. Images acquired between 2012 and 2018. https://www.arcgis.com/home/item.html?id=10df2279f9684e4a9f6a7f08febac2a9 (last visited May. 3, 2023).

Farr, T.G., Rosen, P.A., Caro, E., Crippen, R., Duren, R., Hensley, S., Kobrick, M., Paller, M., Rodriguez, E., Roth, L., Seal, D., Shaffer, S., Shimada, J., Umland, J., Werner, M., Oskin, M., Burbank, D., Alsdorf, D., 2007. The Shuttle Radar Topography Mission. Rev. Geophys. 45 (2) https://doi.org/10.1029/2005RG000183.

Geudtner, D., Torres, R., Snoeij, P., Davidson, M., Rommen, B., 2014. Sentinel-1 System capabilities and applications. In: 2014 IEEE Geoscience and Remote Sensing Symposium: IEEE.

Gorelick, N., Hancher, M., Dixon, M., Ilyushchenko, S., Thau, D., Moore, R., 2017. Google Earth Engine: Planetary-scale geospatial analysis for everyone. Remote Sensing of Environment 202, 18–27. https://doi.org/10.1016/j.rse.2017.06.031.

Grunert, J., Lehmkuhl, F., 2004. Aeolian sedimentation in arid and semi-arid environments of Western Mongolia. In: Paleoecology of Quaternary Drylands. Springer, Berlin, Heidelberg, pp. 195–218.

Grunert, J., Lehmkuhl, F., Walther, M., 2000. Paleoclimatic evolution of the Uvs Nuur basin and adjacent areas (Western Mongolia). Quaternary International 65–66, 171–192. https://doi.org/10.1016/S1040-6182(99)00043-9.

Havivi, S., Amir, D., Schvartzman, I., August, Y., Maman, S., Rotman, S.R., Blumberg, D. G., 2018. Mapping dune dynamics by InSAR coherence. Earth Surf. Process. Landforms 43 (6), 1229–1240. https://doi.org/10.1002/esp.4309.

Hawker, L., Uhe, P., Paulo, L., Sosa, J., Savage, J., Sampson, C., Neal, J., 2022. A 30 m global map of elevation with forests and buildings removed. Environ. Res. Lett. 17 (2), 24016. https://doi.org/10.1088/1748-9326/ac4d4f.

Hugenholtz, C.H., Levin, N., Barchyn, T.E., Baddock, M.C., 2012. Remote sensing and spatial analysis of aeolian sand dunes: A review and outlook. Earth-Science Reviews 111 (3–4), 319–334. https://doi.org/10.1016/j.earscirev.2011.11.006.

Ikazaki, K., 2015. Desertification and a new countermeasure in the Sahel, West Africa. Soil Science and Plant Nutrition 61 (3), 372–383. https://doi.org/10.1080/00380768.2015.1025350.

Klinge, M., Sauer, D., 2019. Spatial pattern of Late Glacial and Holocene climatic and environmental development in Western Mongolia - A critical review and synthesis. Quaternary Science Reviews 210, 26–50. https://doi.org/10.1016/j.quascirev.2019.02.020.

Klinge, M., Lehmkuhl, F., Schulte, P., Hülle, D., Nottebaum, V., 2017. Implications of (reworked) aeolian sediments and paleosols for Holocene environmental change in Western Mongolia. Geomorphology 292, 59–71. https://doi.org/10.1016/j.geomorph.2017.04.027.

Klinge, M. (2001): Glazialgeomorphologische Untersuchungen im Mongolischen Altai als Beitrag zur jungquartären Landschafts-und Klimageschichte der Westmongolei (Aachener Geographische Arbeiten, 35).

Lee, J.-S., Wen, J.-H., Ainsworth, T.L., Chen, K.-S., Chen, A.J., 2009. Improved Sigma Filter for Speckle Filtering of SAR Imagery. IEEE Transactions on Geoscience and Remote Sensing 47 (1), 202–213. https://doi.org/10.1109/tgrs.2008.2002881.

Lehmkuhl, F., 1999. Rezente und jungpleistozane Formungs- und Prozeβregionen im Turgen-Kharkhiraa, Mongolischer Altai. Available online at Die Erde 130, 151–172. https://ci.nii.ac.jp/naid/10009483055/.

Lehmkuhl, F., Grunert, J., Hülle, D., Batkhishig, O., Stauch, G., 2018. Paleolakes in the Gobi region of southern Mongolia. Quaternary Science Reviews 179, 1–23. https://doi.org/10.1016/j.quascirev.2017.10.035.

Lehmkuhl, F., Klinge, M., 2000. Measurements of soil temperatures in the northern Mongolian Altai as indicators for periglacial geomorphodynamic in mountain areas. Zeitschrift für Geomorphologie 44 (1), 75–102. https://doi.org/10.1127/zfg/44/2000/75.

Mahmoud, A.M.A., Novellino, A., Hussain, E., Marsh, S., Psimoulis, P., Smith, M., 2020. The Use of SAR Offset Tracking for Detecting Sand Dune Movement in Sudan. Remote Sensing 12 (20), 3410. https://doi.org/10.3390/rs12203410.

Manzoni, M., Molinari, M.E., Monti-Guarnieri, A., 2021. Multitemporal InSAR Coherence Analysis and Methods for Sand Mitigation. Remote Sensing 13 (7), 1362. https://doi.org/10.3390/rs13071362.

Massei, N., Dieppois, B., Hannah, D.M., Lavers, D.A., Fossa, M., Laignel, B., Debret, M., 2017. Multi-time-scale hydroclimate dynamics of a regional watershed and links to large-scale atmospheric circulation: Application to the Seine river catchment, France. Journal of Hydrology 546, 262–275. https://doi.org/10.1016/j.jhydrol.2017.01.008.

Mullissa, A., Vollrath, A., Odongo-Braun, C., Slagter, B., Balling, J., Gou, Y., Gorelick, N., Reiche, J., 2021. Sentinel-1 SAR Backscatter Analysis Ready Data Preparation in Google Earth Engine. Remote Sensing 13 (10), 1954.

Nashashibi, A.Y., Sarabandi, K., Al-Zaid, F.A., Alhumaidi, S., 2012. Characterization of Radar Backscatter Response of Sand-Covered Surfaces at Millimeter-Wave Frequencies. IEEE Transactions on Geoscience and Remote Sensing 50 (6), 2345–2354. https://doi.org/10.1109/tgrs.2011.2172619.

Pradhan, B., Moneir, A.A.A., Jena, R., 2018. Sand dune risk assessment in Sabha region, Libya using Landsat 8, MODIS, and Google Earth Engine images. Geomatics, Natural Hazards and Risk 9 (1), 1280–1305. https://doi.org/10.1080/19475705.2018.1518880.

Qong, M., 2000. Sand Dune Attributes Estimated from SAR Images. Remote Sensing of Environment 74 (2), 217–228. https://doi.org/10.1016/S0034-4257(00)00112-7.

Reed, M., Stringer, L.C., 2015. Climate change and desertification: Anticipating, assessing & adapting to future change in drylands. Agropolis International, Montpellier. Available online at https://www.idaea.csic.es/sites/default/files/climate%20change%20and%20desertification.pdf.

S.A.M. Saad A.M.A. Seedahmed A. Ahmed S.A.M. Ossman A.M.A. Eldoma COMBATING DESERTIFICATION IN SUDAN: EXPERIENCES AND LESSONS LEARNED. In. Public private partnerships for the implementation of the 2030 Agenda for Sustainable Development 2018 Available online at: https://www.researchgate.net/profile/professor-ahmed/publication/325105898_combating_desertification_in_sudan_experiences_and_lessons_learned.

Shukla, P. R.; Skea, J.; Calvo Buendia, E.; Masson-Delmotte, V.; Pörtner, H.-O.; Roberts, D. C. et al. (2019): IPCC, 2019: Climate Change and Land: an IPCC special report on climate change, desertification, land degradation, sustainable land management, food security, and greenhouse gas fluxes in terrestrial ecosystems. With assistance of Engineering & Physical Science Research Council (EPSRC). Intergovernmental Panel on Climate Change (IPCC). Available online at https://spiral.imperial.ac.uk/handle/10044/1/76618.

Thomas, D.S.G., 2011. Arid zone geomorphology. Process, form and change in drylands, 3. ed., 1. impr. Wiley-Blackwell, Chicester.

Torres, R., Snoeij, P., Geudtner, D., Bibby, D., Davidson, M., Attema, E., Potin, P., Rommen, BjÖrn, Floury, N., Brown, M., Traver, I.N., Deghaye, P., Duesmann, B., Rosich, B., Miranda, N., Bruno, C., L'Abbate, M., Croci, R., Pietropaolo, A., Huchler, M., Rostan, F., 2012. GMES Sentinel-1 mission. Remote Sensing of Environment 120, 9–24.

Turki, I., Laignel, B., Chevalier, L., Costa, S., Massei, N., 2015. On the Investigation of the Sea-Level Variability in Coastal Zones Using SWOT Satellite Mission: Example of the Eastern English Channel (Western France). IEEE Journal of Selected Topics in Applied Earth Observations and Remote Sensing 8 (4), 1564–1569. https://doi.org/10.1109/JSTARS.2015.2419693.

Turki, I., Le Bot, S., Lecoq, N., Shafiei, H., Michel, C., Deloffre, J., Héquette, A., Sipka, V., Lafite, R., 2021. Morphodynamics of intertidal dune field in a mixed wave-tide environment: Case of Baie de Somme in Eastern English Channel. Marine Geology 431, 106381.

Verstraeten, G.; Mohamed, I.; Willems, H.; Laet, V. de; Delgado Blasco, J. M. (2014): Analysis of Aeolian-Fluvial-Human Interactions in the Nile Valley (Central Egypt) by Combining Field-Based Geomorphology with Remote Sensing. In : 34th EARSeL Symposium. 5th European Remote Sensing – New Opportunities for Science and Practice. Abstract and Programme Book. Warsaw, 16-20 June 2014. EARSeL Symposium, Date: 2014/06/16 - 2014/06/20, Location: Warsaw: University of Warsaw (34), p. 55. Available online at https://lirias.kuleuven.be/1739325?limo=0.

Walther, M.; Naumann, S. (1997): Beobachtungen zur Fußflächenbildung im ariden bis semiariden Bereich der West-und Südmongolei (Nördliches Zentralasien) (Stuttgarter geographische Studien, 126).

Williams, K.K., Greeley, R., 2004. Laboratory and field measurements of the modification of radar backscatter by sand. Remote Sensing of Environment 89 (1), 29–40. https://doi.org/10.1016/j.rse.2003.09.006.

Yang, Z., Gao, X., Lei, J., Meng, X., Zhou, N., 2022. Analysis of spatiotemporal changes and driving factors of desertification in the Africa Sahel. CATENA 213, 106213. https://doi.org/10.1016/j.catena.2022.106213.

Zheng, Z., Du, S., Taubenböck, H., Zhang, X., 2022. Remote sensing techniques in the investigation of aeolian sand dunes: A review of recent advances. Remote Sensing of Environment 271, 112913. https://doi.org/10.1016/j.rse.2022.112913.